TRIUMF

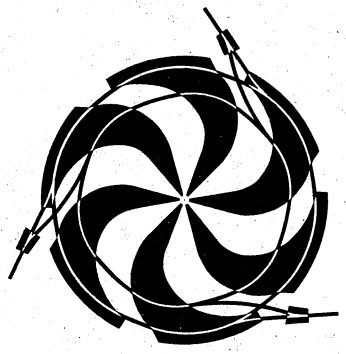

PROGRESS DURING THE FIRST YEAR OF OPERATION OF THE BATHO BIOMEDICAL FACILITY AT TRIUMF

October 1976

R.M. Henkelman, K.Y. Lam, R.W. Harrison, K.R. Shortt, M. Poon, H. Lang, B.W. Jaggi, B. Palcic, and L.D. Skarsgard

Batho Biomedical Facility

and

British Columbia Cancer Foundation

MESON FACILITY OF:

UNIVERSITY OF ALBERTA
SIMON FRASER UNIVERSITY
UNIVERSITY OF VICTORIA
UNIVERSITY OF BRITISH COLUMBIA

TRI-77-2

TRI-77-2

TRIUMF

PROGRESS DURING THE FIRST YEAR OF OPERATION OF THE BATHO BIOMEDICAL FACILITY AT TRIUMF*

October 1976

R.M. Henkelman, K.Y. Lam, R.W. Harrison, K.R. Shortt, M. Poon,
H. Lang, B.W. Jaggi, B. Palcic, and L.D. Skarsgard

Batho Biomedical Facility

and

British Columbia Cancer Foundation

*Work supported by the British Columbia Cancer Foundation
and the National Cancer Institute, Canada

Postal address:

TRIUMF
University of British Columbia
Vancouver, B.C.
Canada V6T 1W5

October 1977

C O N T E N T S

1. INTRODUCTION

The Batho Biomedical Facility at the TRIUMF accelerator is dedicated to an investigation of the efficacy of pion radiation for the clinical management of malignant disease. It has been constructed by the B.C. Cancer Foundation with financial assistance from the Health Resources Fund—under which it has been designated a Health Project of National Significance. A preclinical research programme designed to provide an adequate scientific base from which to initiate treatment is currently in progress, funded by the National Cancer Institute of Canada. Clinical investigation and patient trials will be conducted in collaboration with the Cancer Control Agency of British Columbia, which is responsible for all the management of malignant disease by radiation in the Province.

The period 1974-1976 has witnessed the progression of the TRIUMF biomedical programme from a completely 'paper' project (drawings, computer calculations, purchase orders) to an existing and operational π^- beam with appropriate ancillary support systems and with many of the necessary physical characterizations of the beam completed. Development of much of the equipment and procedures for the residual beam measurements has been completed, particularly for dosimetric measurements of the beam. Studies of ways to control the beam characteristics for delivering specified dose distributions to tumour volumes are at present at an embryonic stage. Initial *in vitro* biological measurements of cell survival as a function of depth have been made.

As a summary of the progress which has been made, a calendar identifying certain landmarks is given in Table I. The schedule of progress is delayed with respect to the anticipated schedule mainly due to three reasons.

Firstly, low carbon magnet steel was extremely difficult to procure in 1971. This resulted in the manufacturer of the two largest magnets failing to supply them and necessitated the procurement of the steel directly by the biomedical group and reletting of the contract. The steel was obtained as a political favour from the Japanese Government by the Government of British Columbia, Department of Trade and Commerce.

Secondly, although TRIUMF had often discussed a beam lines installation and commissioning group, it became clear by the end of 1974 that if the biomedical channel was to be installed, it would have to be done by the scientific personnel of the physical measurements group. Therefore, the whole physical measurements group (and occasionally the biological researchers also) spent approximately six months assembling magnets, measuring magnet fields, surveying, mounting and installing the beam line. Although this resulted in time lost from the scientific programme, it has produced a group of people who have an intimate knowledge of the construction and operation of the beam line. This knowledge has turned out to be invaluable in the solution to more scientific problems involved in the tuning and operation of the beam line. In the long term, the experience gained in the installation of the channel may be regarded as a positive expenditure of time in that the physics group of the biomedical programme have a complete knowledge of their own facility and are not reliant upon accelerator physicists or TRIUMF personnel for the solutions to future tuning or development problems.

Table I. Calendar of important events in the biomedical programme.

1974	Winter	Computer system ordered.	Magnets under construction.
	Spring	Detailed conceptual design of the physical measurements programme completed.	
	Summer	Vacuum designed and constructed.	
	Fall	Shielding designed and contracted. Two-thirds of shielding installed.	
1975	Winter	Magnets delivered. Magnets assembled and surveyed.	
	Spring	Magnets installed and connected. Shielding completed.	
	Summer	June 14, first beam from biomedical channel, proton current < 100 nA.	
	Fall	Cyclotron inoperative due to RF problems. More comprehensive calculations of the channel.	
1976	Winter	First 1 μA beam. Development of particle detection equipment.	
	Spring	Systematic beam line tuning and characterization of particle fluxes.	
	Summer	Development of dosimetric systems and initial measurements.	
	Fall	First 10 μA beam. First *in vitro* biological measurements made.	

Thirdly, since the first operation of the biomedical channel in June 1975 progress on the physical measurements programme has of necessity been correlated with development of the cyclotron. Certain measurements, such as dosimetry and to a certain degree reliable channel tuning, have had to wait until the advent of 1 μA proton beams. Biological irradiations could not be commenced until the availability of greater than 1 μA beams. The progress of the cyclotron to higher intensity, while it has been slower than was anticipated, is quite comparable to the progress made at the other meson facilities, LAMPF and SIN, bearing in mind that the TRIUMF cyclotron became operational only at the beginning of 1975.

Nevertheless, in spite of these delays in schedule, considerable progress has been made by the biomedical group at TRIUMF as will be outlined in the next three sections.

2. DEVELOPMENT OF THE BEAM LINE AND ITS MANAGEMENT

As can be appreciated from the outline above, much of the physics activity in the past three years has been concerned with the beam line. This activity has been predominantly in three areas: development of the beam line; development of a control system; and tuning of the beam line. Progress will be discussed under each of these headings.

2.1 Development of the beam line

The biomedical beam line consists of a line of nine electromagnets consisting of two 45° bending (dipole) magnets, five quadrupole magnets and two sextupole magnets. A drawing of the arrangement of these magnets is shown in Fig. 1. The beam-line plane is inclined at 30° to a horizontal plane to obtain higher fluxes of high-energy pions which are produced at forward directions of the proton beam. The beam line is arranged so that the narrowest dimension of the target is in the direction of the dispersion of the beam momentum, resulting in good momentum resolution in the channel. A short total length of 7.5 m reduces the fraction of pions that decay in flight. A vacuum system along the length of this beam line reduces pion loss due to multiple scattering.

It is clear from the schedule outlined in the introduction that considerable time on the part of the physical measurements group was spent on the actual construction and assembly of the beam line. During this time all the magnets used in the biomedical beam line were magnetically surveyed. Complete field maps of the dipole magnets were measured and the pole faces shimmed to make the actual magnets approximate the ideal sector magnets used in the design calculations. Several measurements of the effective lengths of the dipole magnetic fields were attempted, to bring the computed characteristics of the beam into closer agreement with the actual beam line.

The quadrupole magnets were measured using a rotating coil to determine the harmonic components of the quadrupole field.[1] The effective magnetic centre of two of the quadrupoles was measured using the floating ball technique[2] and was found to be within ±0.03 cm of the geometric centre of the quadrupole. The remaining quadrupoles were aligned, therefore, according to their geometric centres. The field gradients were measured as a function of current in the coils for all magnets in the beam line.

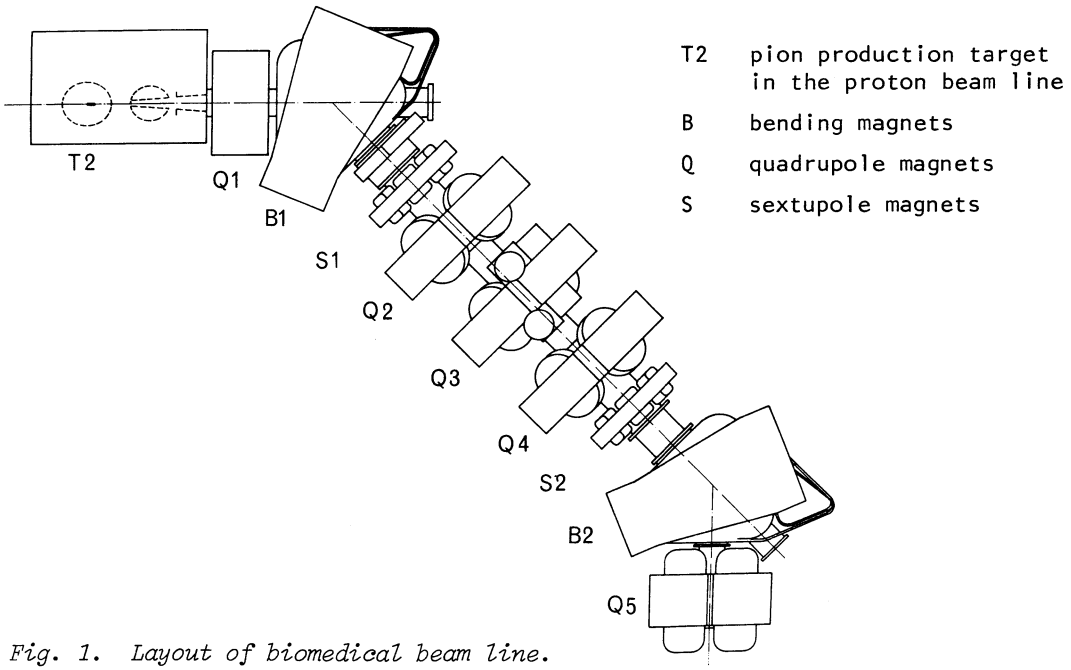

Fig. 1. Layout of biomedical beam line.

The magnets were then assembled in the beam line with the vacuum system. The magnets were positioned on the 30° incline plane to within ±0.06 cm and the angles were controlled to ±10′ arc. The five central magnets were prealigned and installed as a unit. A vacuum system of 7.2 m length, with diameters ranging from 20 cm to 31 cm and including six separate movable apertures and beam interceptors, was installed in the magnet system. Cabling of the power and plumbing of the cooling system were contracted to outside trades.

In June of 1975 the biomedical channel became the first secondary channel at TRIUMF which was ready to accept pions. The channel transmitted its first beam on June 14, 1975.

2.2 Development of a control system

A detailed description of the computer control system of the biomedical channel exists as a TRIUMF internal report TRI-I-75-2 and is available from the authors on request. Therefore, only a general description of the philosophy of the control is included in this report.

The computer system provides two services to the biomedical channel: it is the interface between the wishes of the operator and the execution of those desires on the beam line; and it serves as the collector of large amounts of numerical data from the measurement equipment, presenting these data in intelligible form to the experimenter. Control of the beam line requires the setting of more than 20 individual parameters and determining that these have indeed been correctly set. The computer control system is admirably suited to setting up the beam line to a predetermined set of parameters with much higher reliability than could be expected of the multiple users of the system. It also checks on the status of the beam line once each second and reports deviations from expected behaviour. It provides beam-line status to an operator only as needed, and in a form much more easily understood by the operator than could be achieved without computer control. All these aspects of the beam line control result in a system which is remarkably easy to operate considering its complexity and is suitable for use by a large number of (frequently inexperienced) users. Furthermore, the computer interface with operators protects the beam-line system from unwarranted tampering with the many possible adjustments.

As a data acquisition system, the computer has provided an excellent means for accepting large quantities of numerical data and for controlling the repetitive procedures of beam tuning and beam characterization. The ability to present data graphically is invaluable for the rapid assimilation of information during running time. The ability to carry out procedures under computer supervision has allowed for better utilization of beam time while maintaining a limited number of staff. Examples of the importance of the computer system in both control and experimentation will be elaborated in the subsequent report.

2.3 Tuning of the beam line

In spite of extensive computer calculations of the optical characteristics of a

beam transport system, it is necessary to empirically tune a beam using the calculations as a semi-quantitative guide. Tuning of an evacuated beam line is made more complicated by the non-availability of beam monitors at intermediate positions in the beam line.

A schematic representation of the beam envelope of pion beams of different momenta is shown in Fig. 2. The first dipole magnet B1 disperses the momenta which are then focused by the quadrupole Q2 into a line focus at the mid-plane of the beam line where the movable momentum aperture (slits) can be adjusted to transmit only a given desired range of momenta. The second half of the beam line is symmetric with the first half and serves primarily to superpose the dispersed momenta into an achromatic beam. By varying both the position along the beam axis and field gradient of the final quadrupole Q5, variable field sizes and shapes can be generated from 2 × 2 cm^2 to larger sizes.

The first step in tuning required the generation of a dispersed line focus at the mid-plane. This was done by setting the slits to a narrow width about the mid-line and measuring a differential range curve for the transmitted pions. A differential range curve, measured with plastic scintillators, measures the number of particles stopping as a function of range (depth). An illustration of such a differential range curve is shown in Fig. 3. The largest peak in the vicinity of 13 cm corresponds to the region of stopping pions. The smaller peak at 20 cm is due to the stopping of muons, an inevitable contaminant of pion beams. Since pion beams of different momenta stop at different ranges, a beam composed of a wide band of momenta will exhibit a wide stopping distribution. Conversely, a beam of monoenergetic pions will exhibit a narrow stopping distribution, the width being governed by range straggling of the pions only. Therefore, if a

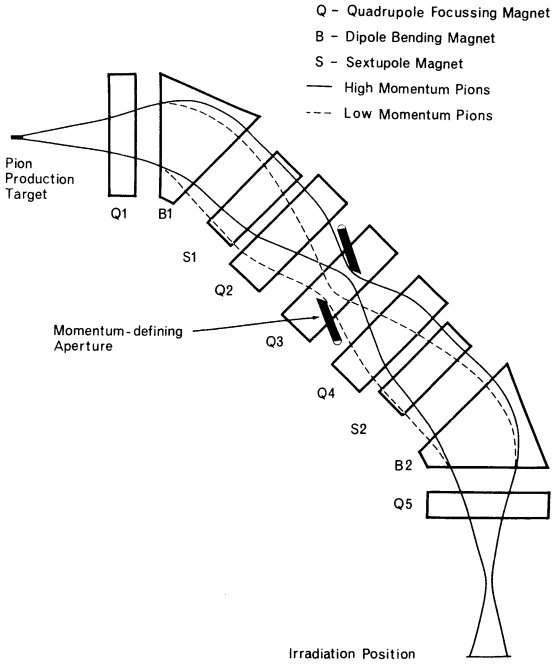

Fig. 2. A schematic presentation of the optical properties of the beam line shows the spatial separation of low- and high-momentum beams at the mid-plane.

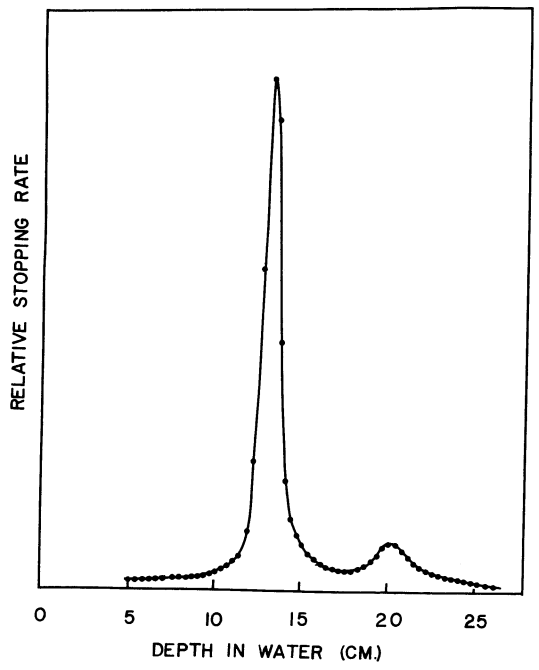

Fig. 3. A differential range curve shows the pion and much smaller muon stopping peaks.

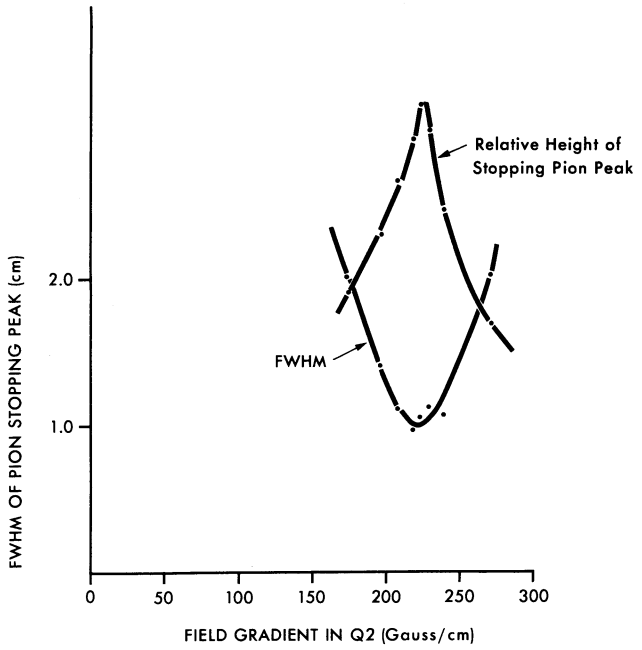

Fig. 4. The FWHM of the pion stopping peak is plotted vs. the field gradient in Q2 showing that it passes through a minimum when Q2 is correctly focused. The relative height of the stopping peak is shown to go through a maximum at the same setting.

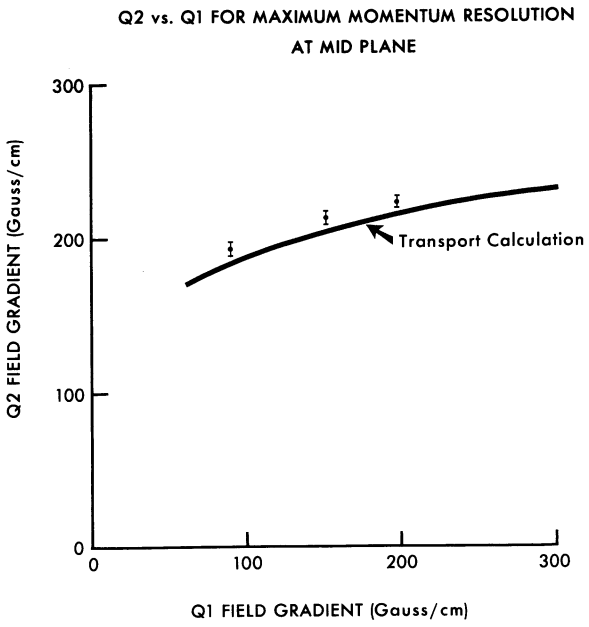

Fig. 5. The experimental setting of Q2 as a function of Q1 for maximum momentum resolution compares qualitatively with the calculated curve.

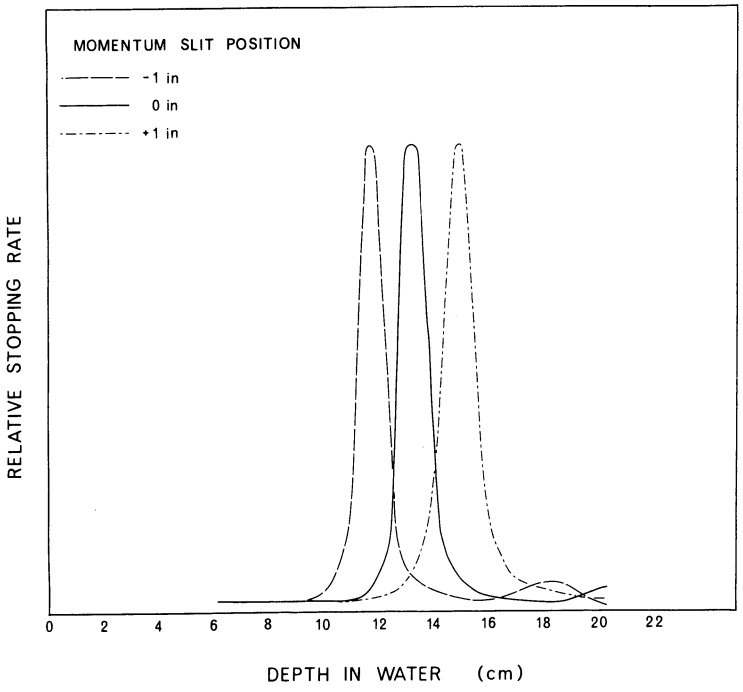

Fig. 6. Three differential range curves show how the range of pions can be adjusted by moving the momentum aperture.

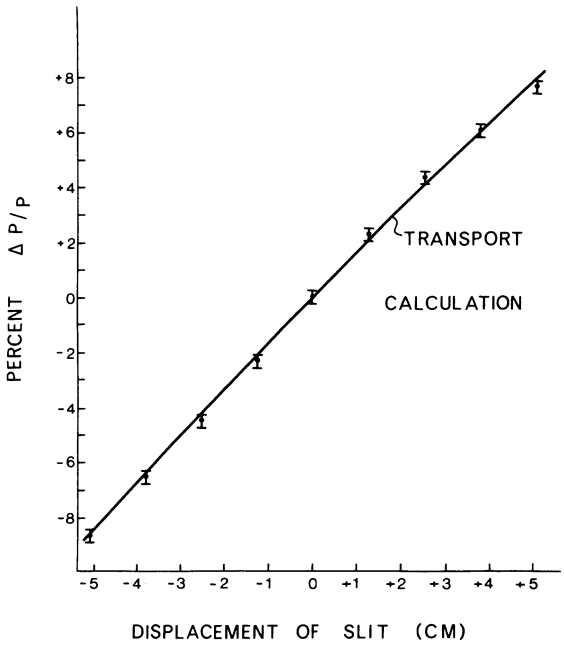

Fig. 7. A comparison of the measured dispersion of the channel with the transport calculation showing excellent agreement.

narrow momentum slit is placed at the mid-plane, a line focus of momentum at this slit will transmit a narrow momentum distribution and hence exhibit a narrow stopping distribution. On the other hand, incorrect focus of Q2, either over-focus or under-focus, will give a beam of wider momentum distribution and hence produce a broader differential range peak. Results of such an experiment are shown in Fig. 4. From this figure it can be appreciated that this experiment provides a very sensitive method for tuning the front half of such a channel. Such an experiment needs to be done for each possible setting of Q1. The resulting Q1 vs. Q2 data for correct focus at the mid-plane are compared with the calculated result in Fig. 5. There is general qualitative agreement although exact agreement in the field gradients is not obtained.

From the minimum achievable width of 1.1 cm it is possible to estimate the momentum resolution of the channel, by removal of the contribution to this width of the counter thickness and range straggling. Such a calculation indicates that the momentum resolution is 1.5% $\Delta P/P$ FWHM.

Once a proper focus at the mid-plane has been obtained, it is important to measure the dispersion (momentum change vs. displacement). Figure 6 shows the resulting differential range curves for a narrow slit at the mid-line and displaced 2.5 cm to either the high-momentum or low-momentum sides of the beam line. The resulting pion range is shifted from 13.3 cm up to 15.0 cm and down to 11.8 cm. A more detailed experiment of this type results in the dispersion curve of Fig. 7 in which the measurements are in excellent agreement with the calculated second-order dispersion.[3]

Tuning of the second half of the channel is done by assuming that the different momenta are all superposed at two positions beyond the end of the channel. This is achieved by selecting different momenta with the blades and then measuring the spatial distribution of the beam at several positions with a multi-wire proportional counter (MWPC). It is then possible, by the adjustment of quadrupoles Q3 and Q4, to obtain the achromatic condition in both slope and displacement at the end of the channel.

Another condition used in tuning is to optimize the flux out of the channel or, equivalently, to maximize the acceptance angle. This involves a conventional optimization of the flux rate in the nine parameter space of the nine current settings of the magnets, making this optimization possible in a reasonable time. Carrying out this optimization has resulted in a 55% increase in flux over the initial channel tune. The particularly sensitive magnets are found to be Q1 and Q3, and thus flux optimization provides a method of determining the otherwise arbitrary setting of Q1.

Tuning of the channel in this manner results in a beam at the exit of the channel when Q5 is off, which is strongly convergent in the plane of the beam line and approximately parallel and of large width in the perpendicular direction. Since this agrees well with the calculated beam slopes, it is a rather simple matter to generate beams of any shape or dimension.

The final two magnets of the beam line are the two sextupoles which are used to remove second-order aberrations in the optics. These are very complicated to use and only very preliminary work has been done to understand them.

3. π^- BEAM MEASUREMENTS

During the time that beam has been available from the biomedical channel a number of physical measurements of the beam characteristics have been made. A summary of those measurements which are closely related to the eventual therapeutic application of the beam are discussed here.

3.1 Beam composition

Because a pion beam is inevitably contaminated with e^- (electrons) and μ^- (mesons), it is necessary to identify the type of particles constituting the beam. After several attempts to do this using pulse height and range discrimination in plastic scintillators, a method based on time of flight was adopted. This is shown diagrammatically in Fig. 8. Instead of using a starting counter at the beginning of the flight path, we use the fact that the accelerator produces protons in pulses every 44 nsec and a few nanoseconds duration. This means that π's, e's and μ's will start out from the target only at discrete and periodic times. Because of the difference in flight time of the same momentum particles of different mass, each particle type will arrive at the end of the beam line at a different time—electrons first, muons next and pions last. By starting a clock on the arrival pulse and timing until the subsequent radio-frequency (rf) pulse, a time distribution distinguishing particle types is obtained, as shown in Fig. 9. In the actual electronics only alternate rf pulses are used as stop signals, resulting in two periods of the time-of-flight spectrum. Integration of the area under the peak of each particle type gives a measure of the number of particles of that type in the flux.

The time-of-flight technique allows an investigation of the fraction of each particle type as a function of channel momentum to be determined. Combining this with the total flux out of the channel as a function of momentum results in the yield curve shown in Fig. 10. Below 130 MeV/c the beam has greater than 50% electrons. The number of electrons falls rapidly with increasing momentum and the number of pions increases rapidly. The π^- and μ^- cannot be distinguished by the time-of-flight method for momenta above approximately 120 MeV/c because the width of the proton pulse exceeds the time separation of the π^- and μ^-. However, calculations show that since the fraction of μ^- is decreasing with momentum the μ^- contamination remains unimportant.

It became apparent very early in the time-of-flight measurements that the fraction of electrons was variable from run to run. This has subsequently been shown to be dependent primarily on the position at which the proton beam strikes the target. An experimental demonstration of this effect is shown in Fig. 11. A theoretical investigation, coupled with the evidence that when positive particles are considered the number of positrons is the same as the number of electrons at each momentum, has led to an understanding of the electron as arising from pair production from γ's which are the decay products of π^0's produced in the target. When the proton beam skims the top of the target there is less material in which the γ's can convert to electron-positron pairs and hence there are less electrons produced. This effect will be used to minimize the high electron flux from the target. Measurements of the electron contamination in a similar channel and target at SIN yield an e/π ratio of 0.21^4 at 150 MeV/c compared with our

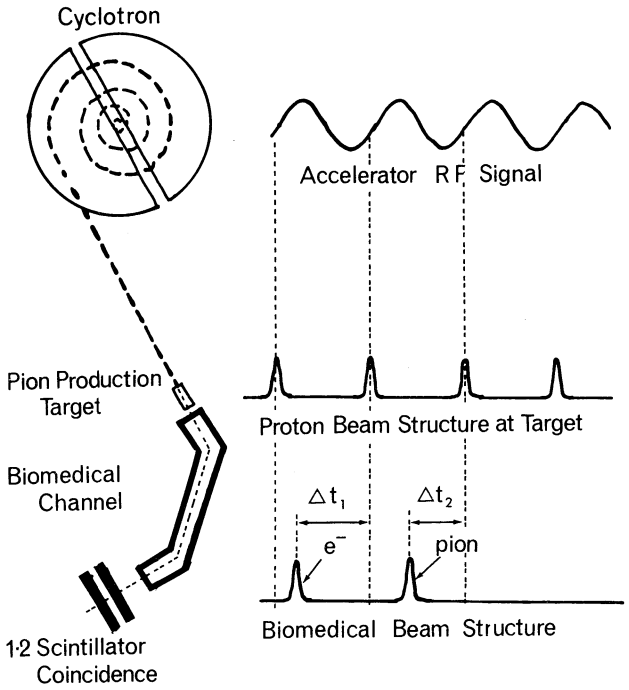

Fig. 8. The time-of-flight technique for particle identification.

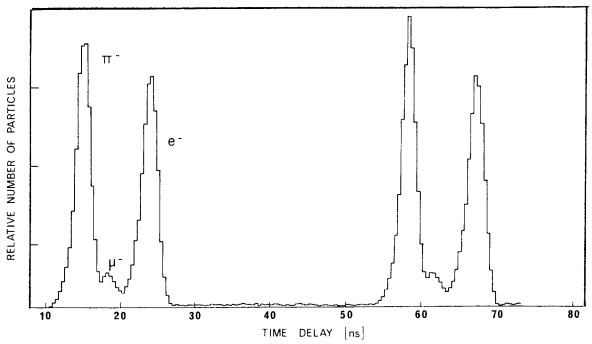

Fig. 9. Time-of-flight spectrum from 150 MeV/c particles from a 10 cm Be production target.

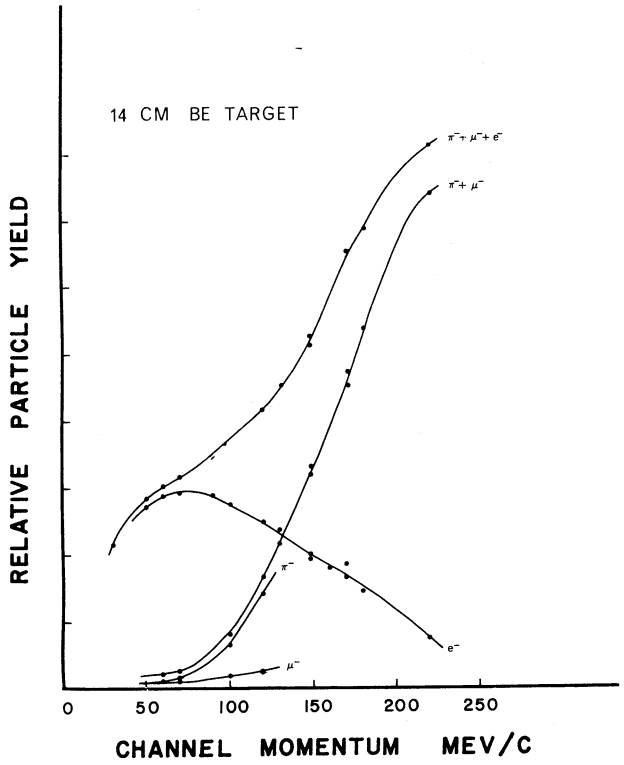

Fig. 10. The relative number of particles leaving the channel is shown as a function of particle momentum. The particle types are distinguished by time of flight.

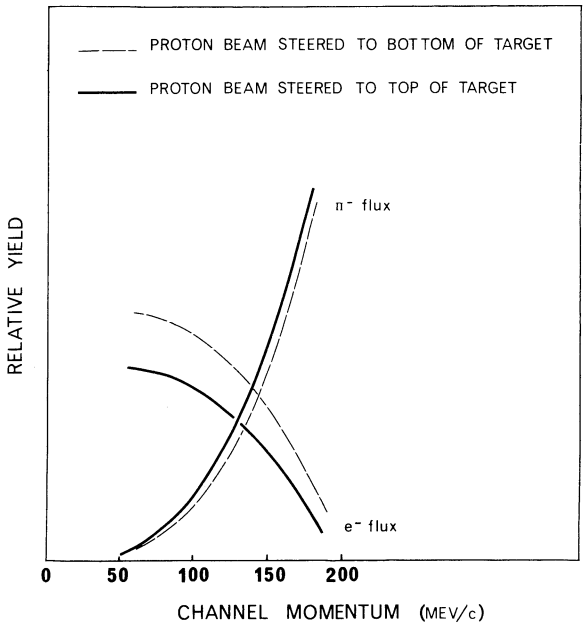

Fig. 11. The effect of producing particles near the surface of the production target shows increased pion fluxes and decreased electron contamination.

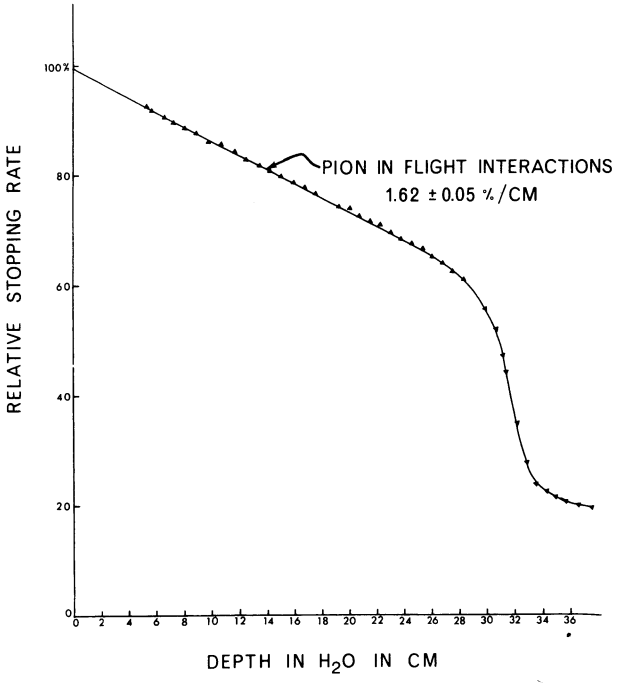

Fig. 12. Integral range curve showing in-flight interactions from a beam of 210 MeV pions.

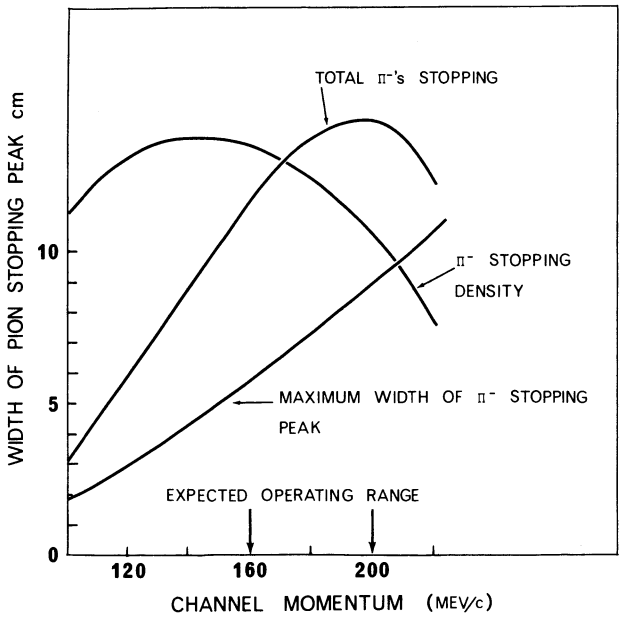

Fig. 13. As a function of channel momentum, the total number of pions reaching the peak, the depth of the range, and the pion stopping density are plotted.

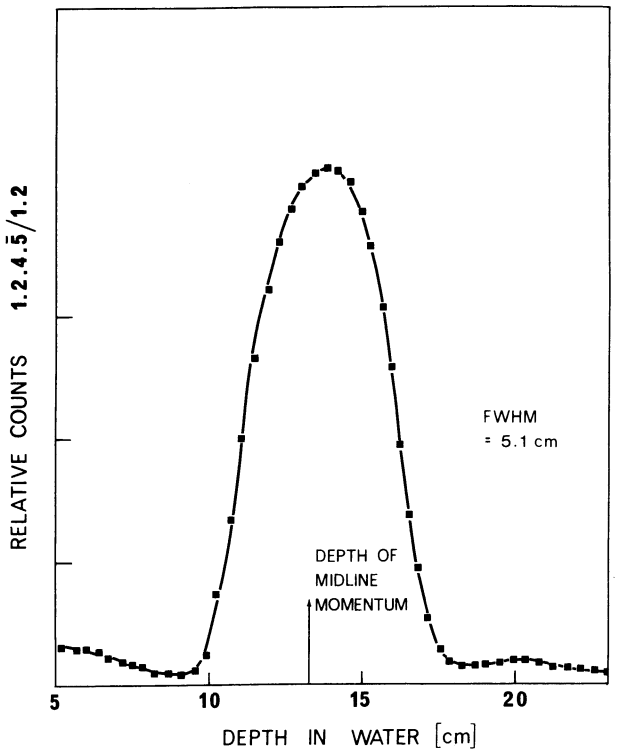

Fig. 14. A differential range curve taken with the momentum slits fully opened showing a stopping width of 5.1 cm FWHM.

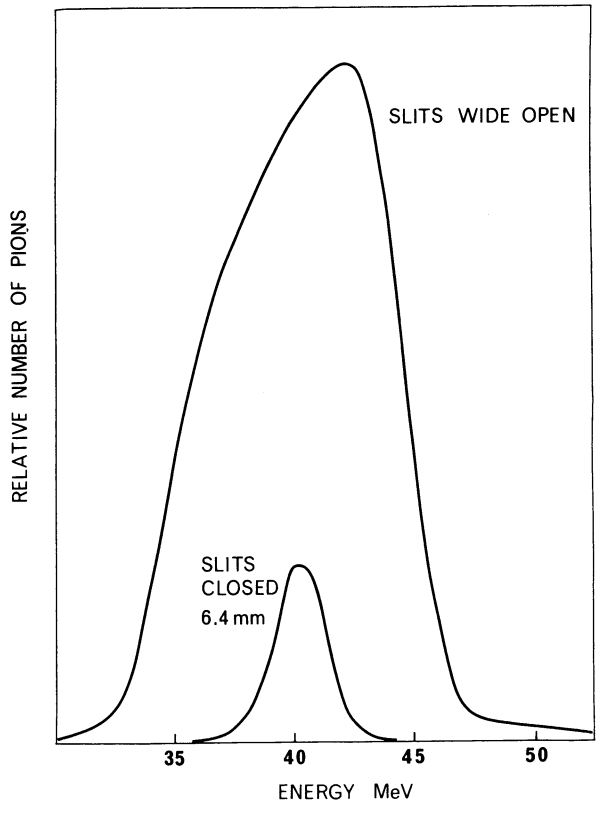

Fig. 15. Energy spectra of positive pions with the momentum slit narrow and with slits wide open.

measurement of 0.66. The differences between the two channels have not yet been satisfactorily reconciled. Since these are very high-energy electrons, minimizing of the electrons is required to reduce the dose beyong the π^- stopping peak.

3.2 In-flight interactions

In spite of the fact that the number of pions continuously increases with increasing channel momentum, the maximum number of pions that reach the stopping distribution is not obtained at the maximum channel momentum, due to the attenuation and large-angle elastic scattering (in-flight interactions) of pions as they pass through water. The in-flight interaction of pions in water has been measured with an integral range curve, and the results are shown in Fig. 12. From such an experiment we deduce the in-flight interaction rate to be 1.62 ± 0.05 %/cm. This rate does not agree with the result reported by Boyd[5] of 2.2 %/cm but is in satisfactory agreement with that of Raju[6] of 1.6 T/g cm^{-2}. The discrepancy may be due to the fact that our experiment was performed with an effectively infinite scintillator so that only elastic scattering of greater than approximately 90° is recorded as an in-flight interaction whereas Boyd's experiment was performed with intermediate-sized counters which identify some elastic scattered events of less than 90° as in-flight interactions.

Combining the in-flight interaction probability with the yield curve allows prediction of the number of pions reaching the stopping region. This is shown graphically in Fig. 13. The total number of pions stopping shows a maximum at 200 MeV/c. However, since a high momentum pion beam of the same percentage momentum acceptance stops over a wider range than a low momentum beam, the relative pion stopping density in number per centimetre is also shown in Fig. 13. The width of the stopping range in centimetres indicated for the measured momentum acceptance of the channel.

3.3 Momentum distribution of the beam

The distribution of pion momenta about the midline momentum of the channel determines the shape of the pion stopping distribution in depth and hence the depth dose profile. The momentum acceptance has been inferred from two kinds of measurements: a differential range curve and a direct measurement of the energy distribution of the particles in the beam.

A differential range curve taken using the maximum acceptance of the channel is shown in Fig. 14. From converting the range directly to momentum without any correction for range straggling, an over-estimate of the acceptance can be calculated to be +7.5% and -6.8% $\Delta p/p$ FWHM. It can also be seen that the acceptance is peaked toward the high momentum side of the midline momentum.

Using a total energy plastic scintillator stopping counter and positive pions, the total kinetic energy distribution of the incident pions can be obtained. Pions are identified by detecting the 4 MeV μ^+ decay in a short interval following the π^+ pulse. The method is described by Axen *et al.*[7] Setting the momentum selection slits to a narrow band about the midline momentum identifies the midline momentum and the resolution of the total energy counter as is shown in Fig. 15. Opening the slits to the full

acceptance gives an energy acceptance from which a momentum acceptance can be deduced as +6.6% and -6.8% $\Delta p/p$ FWHM. Again the distribution is peaked toward the high momentum side. This larger acceptance toward the high momentum side, although not planned, has the advantage of operating relatively uniform stopping distributions and hence fairly uniform doses over the peak of the depth dose profile.

4. DOSIMETRY

Much of the dosimetry apparatus and set-up was tested and calibrated using an X-ray or ^{60}Co unit while the pion beam intensity was still too low. Dosimetry measurements were initiated as soon as the TRIUMF cyclotron could deliver 1 μA of proton current to the pion production target so that some preliminary biological experiments could be started. The various field sizes required for different irradiation experiments necessitated an automatic dosimetry system which was set up to map the dose field of new beam tunes when they are being set up as required. The best available beam tune provides about 20 rad/h/μA of proton from the cyclotron for a volume of about 3 × 3 × 5 cm at the pion stopping region. The progress in the dosimetry measurements can be described in terms of the following systems.

4.1 The dosimeter system

The dosimeter system can be divided into two subgroups: namely, the beam-monitoring dosimeters and measurement dosimeters. The beam-monitoring dosimeters have all been set up, tested and installed. They consist of a transmission chamber and an identical duplicate used as a back-up, which is powered and read independently. In addition, there is a transmission quadrant chamber to monitor the lateral drifting of the beam. All three chambers are mounted together at the exit end of the biomedical channel.

The measurement dosimeters consist of a 0.5 cc sensitive volume Spokas tissue-equivalent chamber, a 2 mm gap, 2 cm diam tissue-equivalent plastic parallel plate chamber, some miniature silicon diodes, and a 0.1 cc EG&G tissue-equivalent plastic thimble chamber. The parallel plate chamber can be pressurized up to 10 atm and is currently being used to study dosimetry using various gases and pressures. The diode system has been developed at the Physics Department of the B.C. Cancer Institute and has a better spatial resolution and higher output than the ionization chambers. Film dosimetry using Kodak X-ray films is also being developed. This is a relatively fast technique and so will be used for routine checking of dose maps. This multiplicity of dosimetric systems will provide a better understanding of the compexities of pion dosimetry.

4.2 The automatic dosimetry system

For detailed planning of irradiation of biological systems, a complete three-dimensional dose map is often required. At a beam intensity of 1 μA protons, it takes on the average about 10 sec to measure the dose to better than 5% accuracy at any location, so a complete three-dimensional dose map which requires thousands of points would take ten to twenty hours. This type of repetitive and tedious measurement is

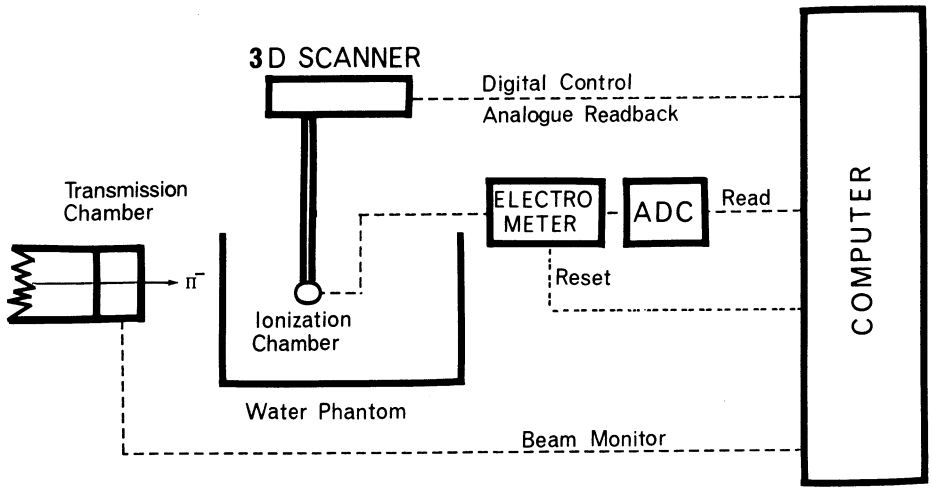

Fig. 16. Schematic representation of the automatic dosimetry system.

best handled by computer automation, and hence an automatic dosimetry system based on on-line computer control has been set up. Figure 16 outlines the apparatus in this system. The radiation dose rate in a water phantom is measured by a dosimeter; the position is controlled by a three-dimensional scanner manufactured by SHM Nuclear, California. The dosimeter used can be any of the ion chambers mentioned, or a silicon diode. The dose rate is measured by an electrometer and an analogue-to-digital converter, and it is scaled against a monitor transmission chamber at the exit of the pion channel.

All the control and data readback are handled by the NOVA II minicomputer via a standard CAMAC[8] computer interface system. The special scanner-computer interface CAMAC module was designed and constructed in our laboratory. The only other CAMAC modules required are a preset counting register and a 10-bit analogue-to-digital converter. This relatively simple automatic system operates reliably and has proven very valuable. Additional computer programming has been developed to handle and display the large amount of data obtained.

4.3 Dosimetry results

Depth dose profiles have been measured with both the Spokas chamber and the parallel plate chamber for a number of different tunes. A depth dose distribution for a nominal 4 cm × 4 cm beam size tune is shown in Fig. 17. The dose in the peak region is relatively flat due to the asymmetry in the momentum acceptance of the channel. Examples of the ability to localize the pion dose peak in depth are shown in Fig. 18 in which a narrow momentum band of pions is used. Using dynamic shaping of the momentum distribution and using the momentum slits during irradiation should make it possible to sharpen up the rise to and fall off from the pion stopping peak. Experimentation of this type has not yet been started.

The automatic dosimetry system has been used to make isodose maps of the beam. This is done by recording the dose at the grid points of a 5 mm × 5 mm grid. Isodose

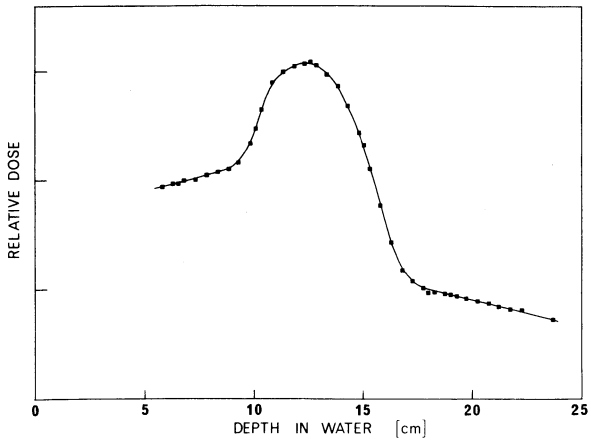

Fig. 17. Depth dose curve with the maximum momentum acceptance of the channel for a midline momentum of 148 MeV/c.

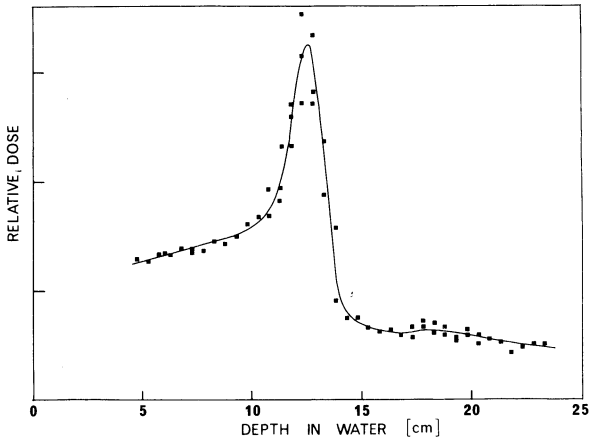

Fig. 18. Depth dose curve measured for a narrow momentum byte using a parallel plate ionization chamber with a 2 mm gap.

contours are drawn in by a computer plotting routine. A total of four maps are made for each tune: two transverse scans of the beam at the entrance to the water phantom and at the dose peak and two longitudinal scans, one in the plane of the beam line (which is at 30° to the horizon) and the last one orthogonal to the beam plane. This system has been at 1 μA of proton beam intensity, only 1% of the final intensity of the facility. This requires approximately 15 sec of integration time at each dose point and thus makes mapping extremely time consuming. However, the dosimetry system operates with sufficient reliability to be left unattended overnight and is able to complete a full map in this time. Figures 19 and 20 shows maps from two tunes which are in use at the biomedical facility. The first was designed to give the maximum possible dose in the minimum lateral volume. Because of multiple scattering, however, pions are scattered in the peak region giving an uncharacteristically low peak-to-plateau ratio on the depth dose profile. The second tune, shown in Fig. 20, is a broader tune. The tune was designed to give a 4 cm × 4 cm uniform field at the stopping region. The square shape of the tune and its inclination at 30° to the horizon can be seen from the transverse scans. It should be noted that this tune is obtained without the use of any collimators and uses only the optics of the beam line. Considerable sharpening of the dose gradients at the edge of the field will in the future be obtained with collimators.

5. *IN VITRO* BIOLOGICAL MEASUREMENTS

During the time since the biomedical channel became operational in June 1975 we have been limited to low-intensity cyclotron beams, generally less than 1% of the design capacity of the cyclotron. As a result, it has not been possible to begin the comprehensive *in vitro* measurements that are planned for the determination of RBE and OER values throughout the π^- dose distribution. However, a few preliminary experiments have been carried out during brief periods of higher beam intensity.

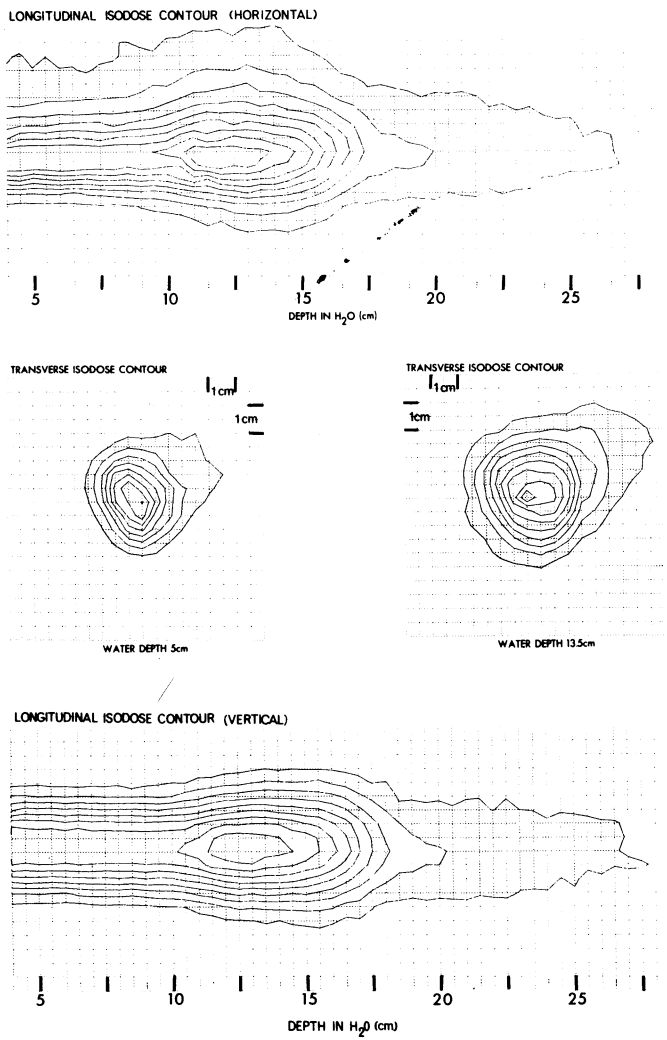

Fig. 19. Isodose maps with contours at 10% intervals for a 148 MeV/c momentum tune with a small spot focus. The radiation field is uncollimated and the full momentum acceptance of the channel is used.

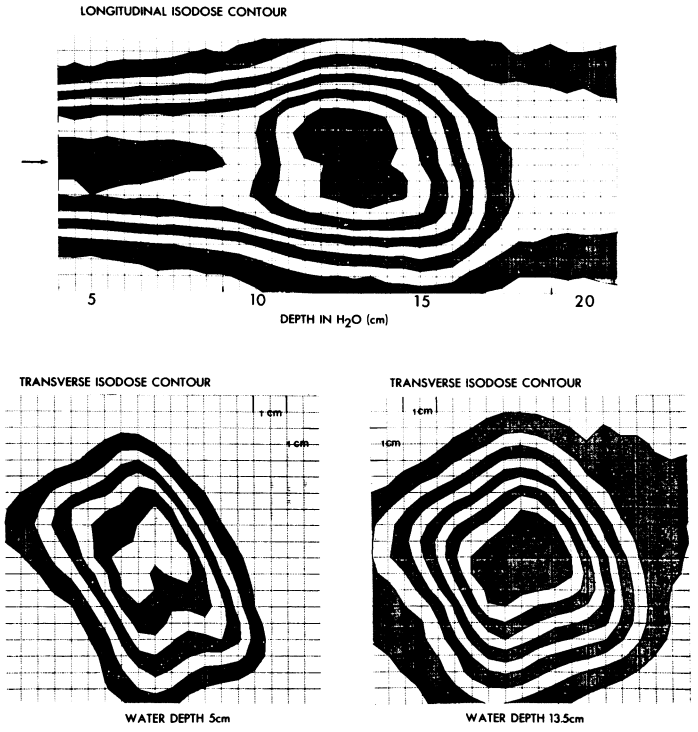

Fig. 20. A similar isodose map for a 148 MeV/c tune with a broader focus. The shape of the spot is due to the optics of the channel since no collimation has been used.

Most of the effort devoted to this project in the past two years has been directed towards the development of new techniques to facilitate rapid and accurate measurement of the radiobiological properties of this complex beam. This has required a wide range of control experiments to ascertain that the new techniques provide meaningful results and to establish the base-line responses for conventional radiations. The following section describes this phase of the program, which is largely complete.

5.1 Development of the gel technique for cell survival measurements

In any particular π^- treatment volume the proportion of the physical dose arising from high LET (linear energy transfer) components will increase with depth as the fraction of the 'star' contribution increases up to the maximum pion range. As a consequence, the RBE will also increase with depth, while the OER will decrease. This situation necessitates a comprehensive series of measurements of RBE and OER values throughout the dose distribution. In order to facilitate this we have developed a system whereby cultured cells are irradiated suspended in a cylinder of 25% gelatin.[9] After irradiation the gel is sliced, individual slices are dissolved and the resulting cell suspension can be diluted and plated, thus allowing cell survival measurements to be made as a function of distance along the axis of the cylinder. This technique is illustrated in Fig. 21 along with results of an experiment designed to test its capacity to resolve sharp changes in dose distribution. In this test the cylinder containing cells suspended in 25% gelatin was irradiated with a sharply defined X-ray beam, the axis of the beam normal to the cylinder. After irradiation (1300 rad) the gel was extruded and sliced with a fine wire

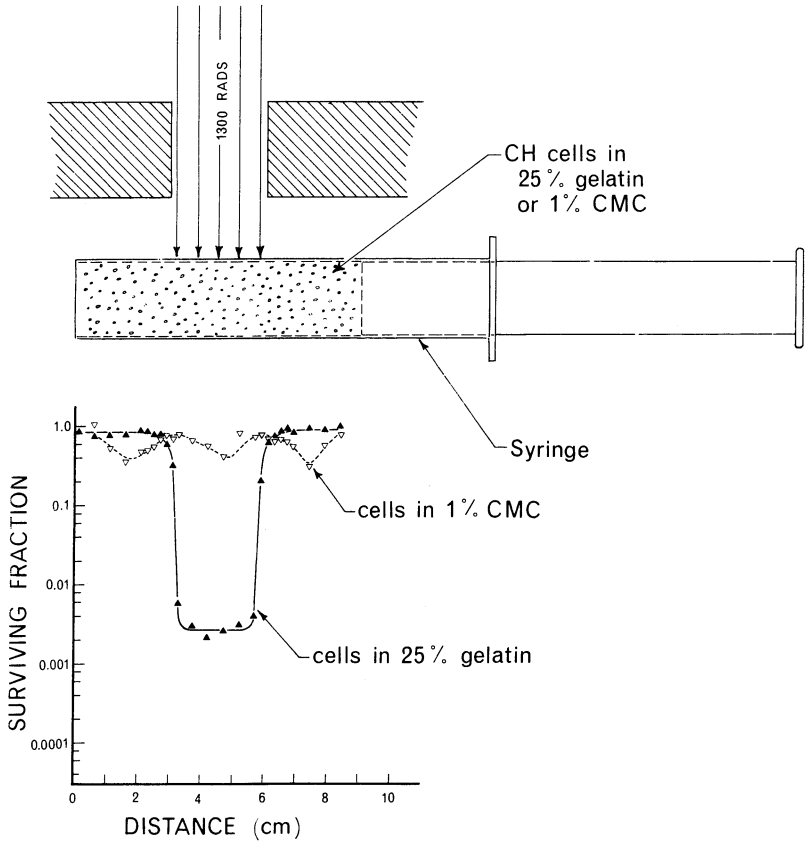

Fig. 21. Illustration of the 'gel' technique developed for the in vitro biological experiments at TRIUMF. Chinese hamster cells ($CH2B_2$) immobilized in 25% gelatin or 1% carboxymethylcellulose (CMC) were irradiated as shown with ^{60}Co γ-rays. The lower half of the figure shows the survival (1300 rad) measured at various positions along the length of the syringe (see text). Closed triangles: cells in 25% gelatin; open triangles: cells in 1% CMC.

at intervals as small as 2 mm and plated for colony formation. The entire slicing procedure requires only 5-10 min. Survival of the Chinese hamster cells ($CH2B_2$) used in this experiment is shown in the lower half of the figure, plotted against distance along the length of the cylinder. It can be seen that survival drops very sharply in the region which was heavily irradiated, and it seems clear that this system has the capacity to easily resolve the dose differences that will be present in a π^- dose distribution.

Also shown in Fig. 21 is the result of a similar experiment where 1% carboxymethylcellulose (CMC) was used instead of 25% gelatin. The resulting viscous fluid (CMC does not form a gel) was extruded through a closed-end syringe and plated for survival. Here the high dose region was not resolved at all, apparently due to mixing of the fluid as it was extruded.

Before one can contemplate using the gelatin system for an extensive series of radiobiological studies with π^- beams, a number of important questions must be answered:

- How well does the elemental composition of the gelatin system reflect the composition of tissue?
- Is gelatin toxic to cultured cells?
- Are radiation responses measured in gelatin representative of *in vitro* responses measured conventionally, i.e. in nutrient medium?
- Can suspensions of cells in gelatin be adequately de-oxygenated to permit oxygen enhancement ratio (OER) determinations?

A good deal of work has gone into providing answers to these questions, answers which are briefly discussed below.

5.1.1 Tissue equivalence

An important consideration in the selection of any experimental system is that the irradiation medium or phantom be tissue equivalent. This is particularly important for π^- beams where, in tissue, most of the star events occur in carbon and oxygen nuclei. Table II shows a comparison of the composition of soft tissue, 25% gelatin and

Table II. A comparison of the composition of soft tissue, 25% gelatin and 1% carboxymethylcellulose

Element	Soft tissue	25% gelatin (in PBS)	1% CMC (in PBS)
H	10.2	10	11.2
C	12.3	12	0.5
N	3.5	4.5	
O	72.9	73	88.4
S,P	0-3		

1% CMC. It can be seen that at a concentration of 25% gelatin (weight/volume) gelatin

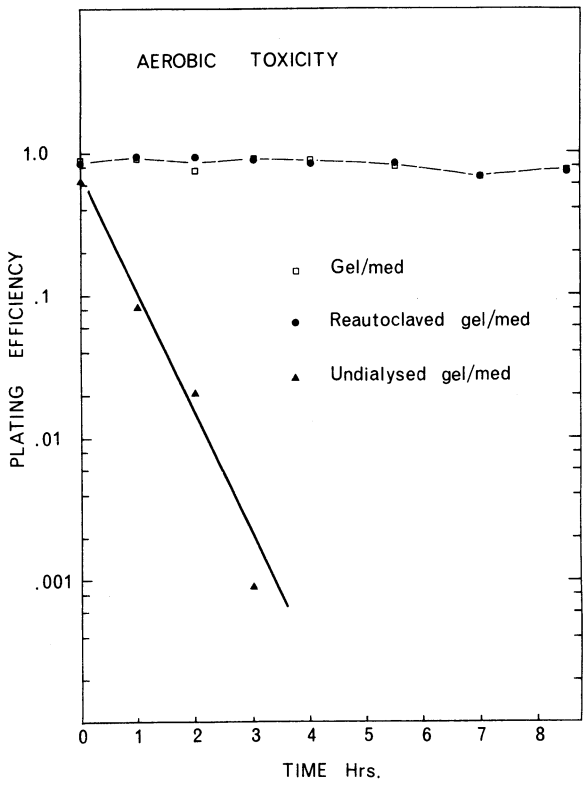

Fig. 22. The toxicity of various gelatin preparations to $CH2B_2$ cells, incubated at 37°C under aerobic conditions. Open squares: dialysed gelatin in medium; closed circles: dialysed gelatin which was reautoclaved before mising with medium; closed triangles: undialysed gelatin in medium. All preparations were 25% gelatin w/v in F-16 medium.

reproduces quite accurately the composition of soft tissue, a fact that is not surprising since gelatin is derived from animal tissue.

5.1.2 Toxicity

Gelatin, as it is received from the supplier (Fisher #G-8), is quite toxic to cultured cells. If it is sterilized and added to medium, it reduces the plating efficiency of $CH2B_2$ cells to 10% in about one hour, as can be seen in Fig. 22, the undialysed gel/med curve. We have shown, however, that this toxicity can be almost entirely removed by extensive dialysis of the gelatin against phosphate-buffered saline (PBS), as can be seen from the curve in Fig. 22 labelled 'gel/med'. This preparation can also be reautoclaved without introducing any additional toxicity. The gelatin preparation which we routinely use now, designated 'gel/med', is 25% gelatin in the appropriate nutrient medium.

5.1.3 Survival in gel vs survival in medium

In order to determine whether the large amount of protein present in gelatin might alter the radiation response of cells suspended in it, parallel survival responses were measured in gel/med and in nutrient medium, using cells from the same culture population for both tests. The data of Fig. 23 are the results of such an experiment using Chinese hamster ovary (CHO) cells. In this experiment the samples were at room temperature, 22°C, during irradiation, with the result that the gel/med samples were in the gel state, as they will be for pion beam experiments. There is no significant difference between the responses measured in gel/med or in regular medium as can be seen from these data. Similar results were obtained for $CH2B_2$ cells.

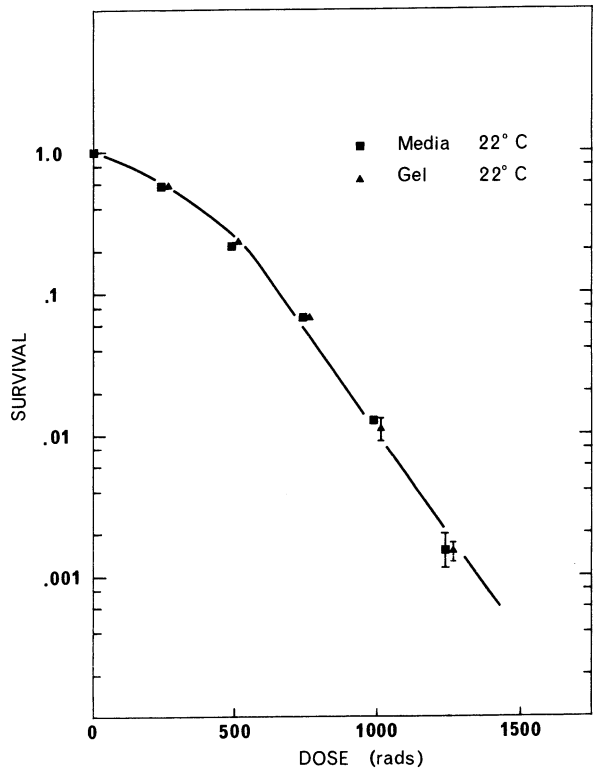

Fig. 23. Comparison of the γ-radiation response of CHO cells at 22°C measured (i) in nutrient medium: closed squares; and (ii) in gel/med (25% gelatin in MEM-F-16 medium): closed triangles. Note that the triangles have been displaced to the right and the squares to the left of the true dose to allow better visualization of the very similar survival values. Standard errors are indicated by error bars except for those cases where the error bars are smaller than the plotting symbol.

Furthermore, it has been shown that there is no difference between the survival responses of cells in gelatin at either 22°C or 37°C as is the case for cells in medium.

5.1.4 OER measurements in gel/med

Since we wish to use the gelatin system for OER determinations at various positions in the π^- dose distribution, it was necessary to determine whether one could obtain the necessary state of hypoxia in a gel/medium cell suspension. For these studies, suspensions of cells in gel/med were gassed and irradiated at 37°C in the same glass vessels that we use for our radiosensitizer studies,[10] which provide for continuous agitation of the suspension so that effective gas substitution can be achieved. Such suspensions were gassed with nitrogen or oxygen for 1-1½ h at 37°C prior to irradiation. Figure 24 shows the survival responses measured under aerobic and hypoxic conditions. The OER in this experiment is 2.8, comparable to the OER which we observe in cells suspended in medium. Thus it appears that one can achieve a level of hypoxia in the gel system adequate for OER determinations.

From these control studies it appears that the gelatin system which we have developed provides a very appropriate and efficient technique for the *in vitro* preclinical studies. It has, incidentally, been adopted by groups at LAMPF, Stanford and SIN, and we have supplied to these groups our detailed procedures for its use.

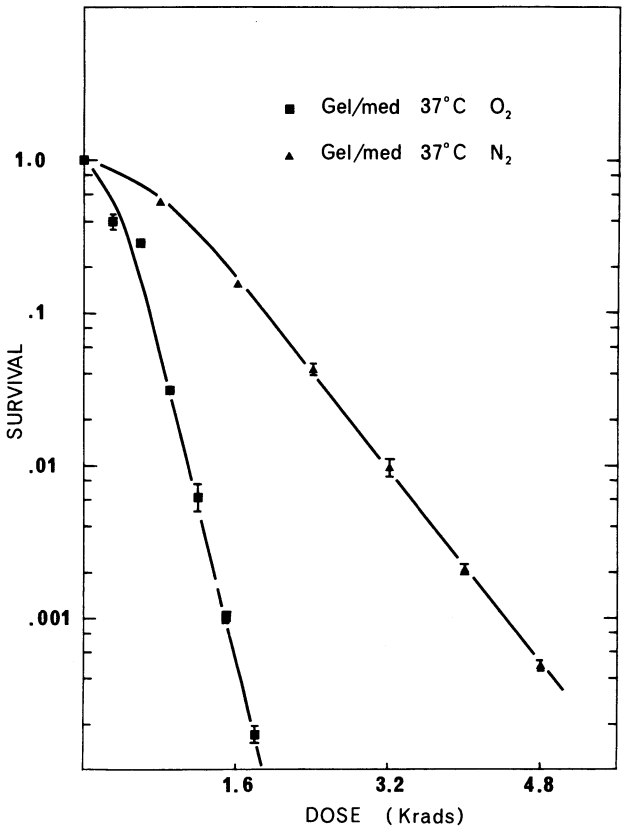

Fig. 24. Survival of $CH2B_2$ cells γ-irradiated at 37°C in gel/med (25% gelatin in MEM F-16 medium) under aerobic conditions (closed squares) and under hypoxic conditions (closed triangles). The OER from these responses is 2.8.

5.2 Cell survival results

On March 23, 1976 the proton beam at TRIUMF was raised to 5 μA for 1.5 h for the purpose of radiation safety measurements. This afforded us the first opportunity to attempt some π^- radiobiology, and consequently we irradiated a cylinder of $CH2B_2$ cells suspended in gel/med. Figure 25 shows the resulting survival vs depth profile along with the depth dose profile for the beam that was used. The estimated dose at the peak was 140 rad, a very small dose for definitive survival measurements. About all that one can say about this result is that the decrease in survival coincides with the peak in the dose distribution.

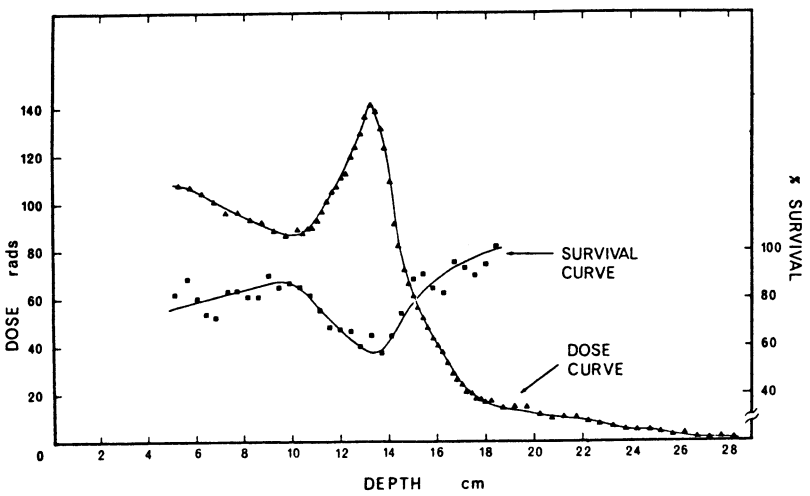

Fig. 25. The first radiobiological experiment at TRIUMF. The survival of $CH2B_2$ cells, irradiated with a peak π^- dose of approximately 140 rad, is plotted as a function of depth in water. The cells were irradiated at 0°C, suspended in a cylinder of gel/med (25% gelatin in MEM F-16 medium). The survival is a minimum at or just beyond the dose maximum, also plotted in this figure. π^- beam characteristics: 148 ± 9 MeV/c, stopping peak at 13.3 cm, 3 × 3 cm field.

Subsequent measurements using 10 μA test runs and a better pion beam time (actually the time shown in Fig. 20) have allowed more reliable measurements of the cell survival at depth to be made. The results of these measurements at two different peak dose values are shown in Fig 26. Work continues with the availability of higher intensity beams on the *in vitro* biological characterization of pion radiation field. From these preliminary measurements it can be concluded that the biological properties of the pion radiation differs little from the predicted characteristics.

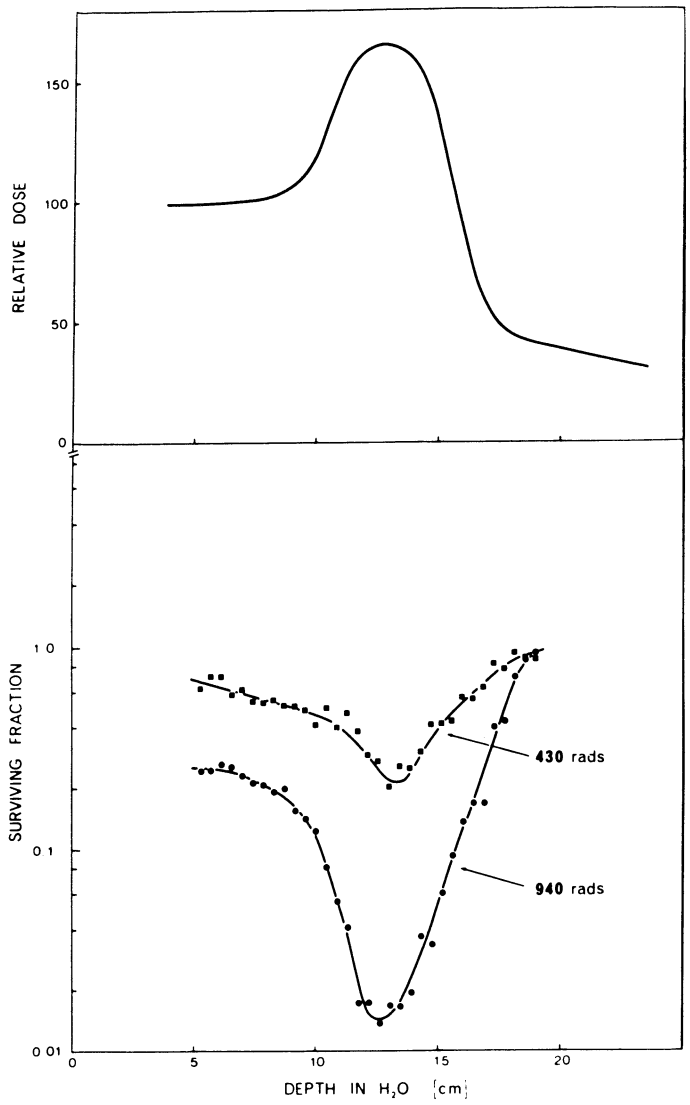

Fig. 26. Survival of Chinese hamster cells ($CH2B_2$) π^--irradiated in 25% gel/medium. Top: The depth dose profile of the pion beam (138-158 MeV/c). Bottom: Survival profiles for cells irradiated in gel/medium at 0°C. Dose rate at peak approximately 2 rad/min. Control plating efficiency 70%.

6. SUMMARY

Much of the work of preparing a pion beam at TRIUMF for clinical radiotherapeutic trials has now been done. Active work continues on the physics and dosimetry systems. *In vitro* biological characterization of the pion radiation continues whenever at least 10 μA beams are available. *In vivo* biological systems (not described in this report) have been prepared and tested using ^{60}Co radiation as a control. These experiments will begin at TRIUMF with the availability of a 30 μA proton beam. It is expected to begin clinical investigations approximately six months after the availability of 100 μA beams. This sets a date for the initiation of clinical investigation in mid-1978.

REFERENCES

1. J.K. Cobb and D. Horelick, 'A new precision measurement system for beam transport type magnets', Proc. 3rd Int. Conf. on Magnet Technology, Hamburg, 1970 (DESY, Hamburg, 1970), p.1439.
2. R.W. Cobb, T.A. Hodges, A.D. Kirk, R.M. Pearce and L.P. Robertson, 'Method for finding the magnetic centre of a quadrupole field', Nucl. Instr. & Meth. 106, 259 (1973).
3. K.L. Brown and S.K. Howry, 'Transport-360', Stanford Linear Accelerator report SLAC-91 (1970).
4. H. Appel, V. Bohmer, G. Buche, W. Kluge and H. Matthay, 'π^--beam studies using time-of-flight methods', Atomkernenergie (ATKE) 27, 177 (1976).
5. D. Boyd, 'Pion depth-dose distribution including the effect of interactions in flight', High Energy Physics Laboratory, Stanford University report TN-71-1 (1971).
6. M.R. Raju and C. Richman, 'Negative pion radiotherapy: physical and radiobiological aspects', Radiation Research Quarterly 8, 159 (1972).
7. D. Axen, G. Duesdieker, L. Felawka, C.H.Q. Ingram, G. Jones, M. Salomon and W. Westlund, 'A high-resolution scintillation counter with particle identification for use with pions', Nucl. Instr. & Meth. 118, 435 (1974).
8. H-J Stuckenberg, CAMAC Bulletin, Issue No. 13, Supp. A, September 1975.
9. L.D. Skarsgard and B. Palcic, 'Pretherapeutic research programmes at π^- meson facilities', Proc. XIIIth Int. Congress of Radiology (Madrid, October 15-20, 1973), International Congress Series No. 339, Radiology, Vol. 2, p.447. Exerpta Medica, Amsterdam, A74.
10. L. Parker, L.D. Skarsgard and P.T. Emmerson, 'Sensitization of anoxic mammalian cells to x-rays by triacetoneamine N-oxyl: Survival and toxicity studies', Rad. Research 38, 493 (1969).